Label-Free Composition Analysis of Supramolecular Polymer – Nanoparticle Hydrogels by Reversed-Phase Liquid Chromatography Coupled with a Charged Aerosol Detector

Shijia Tang a,#,*, Zachary Pederson a,#, Emily L. Meany b, Chun-Wan Yen a, Andrew K. Swansiger c, James S. Prell c, Bifan Chen A, Abigail K. Grosskopf f, Noah Eckman c, Grace Jiang b, Julie Baillet d, Jackson D. Pellett a, Eric A. Appel d,*

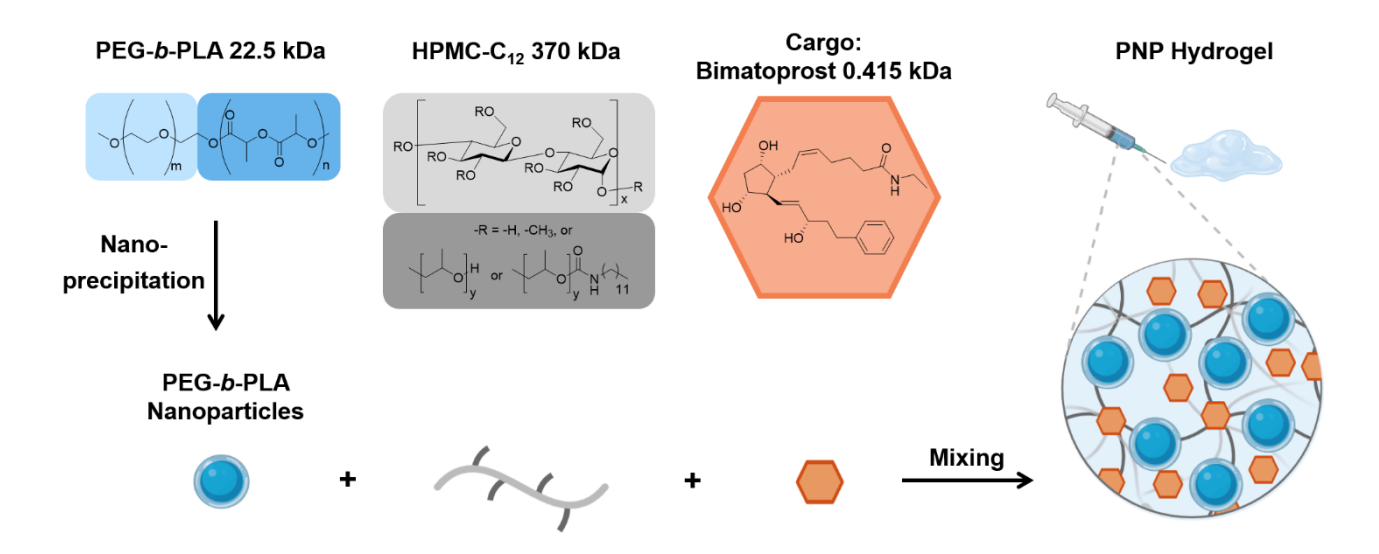
- ^a Synthetic Molecule Pharmaceutical Sciences, Genentech, Inc., South San Francisco, CA 94080, USA
- ^b Department of Bioengineering, Stanford University, Stanford, CA 94305, USA.
- ^c Department of Chemical Engineering, Stanford University, Stanford, CA 94305, USA.
- ^d Department of Materials Science and Engineering, Stanford University, Stanford, CA 94305, USA.
- ^e Department of Chemistry and Biochemistry, University of Oregon, Eugene, Oregon 97403, USA
- ^f Preclinical and Translational Pharmacokinetics and Pharmacodynamics, Genentech, Inc., South San Francisco, CA 94080, USA

ABSTRACT: Supramolecular hydrogels formed through polymer-nanoparticle interactions are promising biocompatible materials for translational medicines. This class of hydrogels exhibits shear-thinning behavior and rapid recovery of mechanical properties following applied stresses, providing desirable attributes for formulating sprayable and injectable therapeutics. Characterization of hydrogel composition and loading of encapsulated drugs is critical to achieving desired rheological behavior as well as tunable in vitro and in vivo payload release kinetics. However, quantitation of hydrogel compositions is challenging due to material complexity, heterogeneity, high molecular weight, and the lack of chromophores. Here, we present a label-free approach to simultaneously determine hydrogel polymeric components and encapsulated payloads by coupling a reversed phase liquid chromatographic method with a charged aerosol detector (RPLC-CAD). The hydrogel studied consists of modified hydroxypropylmethylcellulose, selfassembled PEG-b-PLA nanoparticles, and a therapeutic compound, Bimatoprost. The three components were resolved and quantitated using the RPLC-CAD method with a C4 stationary phase. The method demonstrated robust performance, applicability to alternative cargos (i.e. proteins), and was suitable for composition analysis as well as for evaluating in vitro release of cargos from the hydrogel. Moreover, this method can be used to monitor polymer degradation and material stability, which can be further elucidated by coupling the RPLC method with (1) multi-angle light scattering detector (RPLC-MALS) or (2) high resolution mass spectrometry (RPLC-MS) and a Fourier-transform based deconvolution algorithm. We envision this analytical strategy could be generalized to characterize critical quality attributes of other classes of supramolecular hydrogels, establish structure-property relationships, and provide rational design guidance in hydrogel drug product development.

Supramolecular hydrogels are physically cross-linked viscoelastic biomaterials that are rapidly expanding in drug delivery, cell therapy, surgical coatings, medical device applications, and beyond. 1-10 Through tuning the chemistries and crosslinking density (mesh size of a hydrogel molecular network), hydrogels can be made that adopt vastly different chemical or physical properties and can encapsulate a variety of cargoes and accommodate different targeted release time frames. 3, 6, 7 In comparison to chemically cross-linked hydrogels, supramolecular hydrogels rely on physical, noncovalent interactions such as ionic interactions, hydrophobic interactions, hydrogen-bonding, metal-ligand complexation, host-guest complexation, or biorecognition, which provide several clinical and process development benefits, such as gelation without reactive moieties or volume change. 1, 6, 10 Moreover, the reversible, non-covalent interactions in supramolecular hydrogels form dynamic and transient crosslinks, resulting in rapid self-healing and shear-thinning properties that make these hydrogels an ideal formulation strategy for sprayable and injectable therapeutics. ^{6, 7}

While the materials library of supramolecular hydrogels is expanding, few analytical methods have been developed to characterize the critical quality attributes (CQAs) of hydrogels such as drug loading, polymer compositions, and release profiles of the loaded drugs and polymers. Such attributes are important to establish hydrogel structure-property relationships and gain understanding of the gelation process. For example, comparing polymer and drug release profiles simultaneously can shed light on the release mechanisms (i.e., driven by diffusion, erosion), pharmacokinetics, fate of the matrix polymers over time, and establish *in vitro* and *in vivo* correlation (IVIVC), thereby enabling the rational design of hydrogels for specific target product profiles. ³

Scheme 1. Supramolecular Polymer-Nanoparticle Hydrogel Composition and Gelation Process



Several challenges are inherent to the composition analysis of supramolecular hydrogels. From a chromatography perspective, hydrogels often contain both encapsulated payloads and two or more high molecular weight and heterogeneous polymeric components as the gel matrix. This requires a method that resolves multiple components while allowing good recovery for the polymers. In addition, an appropriate sample extraction procedure is critical to dissociate the supramolecular hydrogels and fully extract the individual components without degradation. As a result of these challenges, only the active payload is typically quantitated in hydrogel products to determine drug loading and release profiles. 11, 12 Hydrogel degradation has been monitored gravimetrically (weighing residual gel matrix), which provides limited information about the release of individual polymers and/or chemical changes (i.e. molecular weight, degradation). ¹¹⁻¹³ From a detection perspective, the encapsulated payloads are often UV active, while many polymers lack UV chromophores and require derivatization or an alternative detection principle to quantify. Labeling approaches, such as modifying the polymeric components with fluorescent tags or encapsulating fluorescent dyes as payload surrogates, have been developed for tracking the release of polymers and payloads from hydrogels. 14-20 However, labeling approaches can complicate hydrogel chemistries and/or release kinetics depending on the degree of modification and the properties of the fluorescent modifiers. Tracking fluorescence intensity may not fully reflect chemical changes in the polymer backbones over time. Identifying a label-free approach that combines chromatography separation with a universal detection technique for non-UV absorbing compounds would be beneficial to realize quantitation for all components in a supramolecular hydrogel and capture key chemical changes over time. However, label-free composition analysis of supramolecular hydrogel is rarely explored in the literature, and it remains a gap on what chromatographic separation modes and detection techniques can provide sufficient sensitivity, resolution, and recovery for all the components undergoing quantitative analysis.

Recently, a supramolecular hydrogel platform employing polymer-nanoparticle interactions between dodecyl-modified hydroxypropylmethylcellulose (HPMC-C₁₂) and poly(ethylene

glycol)-block-poly(lactic acid) nanoparticles (PEG-b-PLA NPs) has been developed, which demonstrates injectability and rapid self-healing properties (Scheme 1). ²¹⁻²⁶ These materials are denoted as PNP-X-Y, where X refers to the weight percent loading of the HPMC-C₁₂ component and Y refers to the weight percent loading of the PEG-b-PLA NP component (e.g., PNP-2-10 gels comprise 2 wt% HPMC-C₁₂ and 10 wt% PEG-b-PLA NPs).

In this study, we use PNP-2-10 hydrogel as a model system to develop a label-free analytical method utilizing reversed phase liquid chromatography coupled to a charged aerosol detector (RPLC-CAD) which quantitates all components in the hydrogel—HPMC-C₁₂, PEG-b-PLA NPs, and an encapsulated therapeutic payload, Bimatoprost. A C4 reversed phase column was selected to provide specificity, sensitivity, and recovery for all the hydrogel components. Due to the lack of UV chromophores on both polymeric components, a highly sensitive aerosol-based detection technique, CAD, was identified as most suitable to couple with the RPLC separation for quantitative analysis instead of differential refractometer or light scattering techniques. Beyond quantitation, the RPLC-CAD method was capable of differentiating polymer integrity after degradation or E-beam sterilization and could be combined with multi-angle light scattering (RPLC-MALS) or mass spectrometry (RPLC-MS) for further structural elucidation and monitoring of material stability. The method was also applicable to an alternative cargo, Bovine Serum Albumin (BSA), and demonstrated that this methodology can be generalized to characterize supramolecular hydrogels with various modalities of payloads. Our method demonstrated a label-free approach for composition analysis, characterizing degradation, and release profiles of supramolecular hydrogels, all of which are critical quality attributes.

EXPERIMENTAL SECTION

Materials and Reagents: USP grade HPMC, N,N-diisopropylethylamine, diethyl ether, hexanes, acetone, dimethyl sulfoxide (DMSO), dimethylformamide (DMF), acetonitrile (MeCN), N-methyl-2-pyrrolidone (NMP), diazobicylcoundecene (DBU), acetic acid, formic acid,

monomethoxy-PEG (5 kDa), and 1-dodecyl isocynate were purchased from Sigma-Aldrich and used as received for polymers, nanoparticles, and hydrogel preparation. Lactide (LA) was purchased from Sigma-Aldrich and purified by recrystallization in ethyl acetate with sodium sulfate. Dichloromethane (DCM) was purchased from Sigma-Aldrich and further dried via cryo distillation. For SEC and RPLC analysis, deionized water was obtained from an in-house Milli-Q water filtration system. Acetonitrile (MeCN) and Tetrahydrofuran (THF) were purchased from JT Baker, and LC-MS grade trifluoroacetic acid (TFA) was purchased from Fisher Scientific. DMSO was purchased from Alfa-Aesar. Pullulan standards were purchased from Polymer Standards Service. BSA was purchased from Thermo Fisher Scientific and Bimatoprost was sourced from Toronto research chemicals.

Preparation of PNP Hydrogels: PNP-2-10 hydrogels were formulated (2 wt% HPMC-C₁₂ and 10 wt% PEG-*b*-PLA NPs) according to the previous study. ²⁶ HPMC-C₁₂ was dissolved in PBS at 6 wt% and loaded into a luer-lock syringe. A 20 wt% solution of NPs in PBS was diluted with additional PBS, containing Bimatoprost at the desired concentration, and loaded into a separate luer-lock syringe. The nanoparticle syringe was then connected to a female-female luer-lock elbow and the solution was moved into the elbow until visible at the other end. The HPMC-C₁₂ syringe was then attached to the other end of the elbow with care to avoid air at the interface of HPMC-C₁₂ and the NP solution. The two solutions were mixed for 1 minute or until a homogenous hydrogel was formed. After mixing, the elbow was removed and a needle of the appropriate gauge was attached.

Instrumentation: The RPLC-CAD and SEC-CAD analysis used an Agilent 1260 series HPLC (Agilent Technologies, Santa Clara, CA) equipped with a quaternary pump, vacuum degasser, temperature controlled autosampler, thermostatted column compartment, diode array detector, and coupled to a Thermo Dionex Corona Veo RS CAD detector (Thermo Fisher Scientific, Waltham, MA). For all analysis, CAD evaporation temperature was set to 35°C, data collection was set to 5 Hz, and filter was set to 3.6 seconds.

Chromatographic Conditions for RPLC-CAD: The final optimized RPLC method used the Halo 400 Å C4 column. MPA was 0.05% TFA (v/v) in water and MPB was MeCN. Flow rate was 0.5 mL/min and column temperature was 60 °C. The sample diluent was 25% MeCN in water (v/v) unless otherwise stated. The final method gradient program was as follows: 0 – 2 min, initial hold at 25% MPB, 2 – 5 min, linear ramp from 25% to 80% MPB, 5 – 10 min, hold at 80% MPB, 10 – 11 min, linear ramp from 80% to 98% MPB, 11 – 15 min, hold at 98% MPB then the gradient was brought back to the original condition. The thermostat temperature was set at 60 °C except for E-beam experiment that conducted at 50 °C.

PEG-b-PLA standards were prepared by dissolving solid PEG-b-PLA polymer in MeCN at 1-2.5 mg/mL, then diluting with water and/or MeCN to achieve the desired concentration. In the diluent, the PEG-b-PLA formed nanoaggregates and was denoted as PEG-b-PLA Agg (Figure S1, S2, Supporting Information). HPMC-C₁₂ standards were prepared by adding solid HPMC-C₁₂ to 25% MeCN in water (v/v), then stirring until dissolved (1-2 hrs). Hydrogel samples were dissolved using the step-wise dilution as discussed in the **Diluent Study** section.

The chromatographic data was processed and analyzed in Empower (Waters, Milford, MA). Second order polynomial fitting was used for quantitation analysis against a multi-point calibration standard for each component.

Chromatographic Conditions for RPLC-MS: For MS analysis, an Agilent 1290 series HPLC (Agilent Technologies, Santa Clara, CA) equipped with a binary pump, vacuum degasser, temperature controlled autosampler, thermostatted column compartment, and a diode array detector, was coupled to an Agilent 6545XT qTOF. Chromatography condition used the final method described above. Mass spectra were collected from 360-12000 m/z at a rate of 3 scans/sec. The AJS source was set at a drying temperature of 325 °C, a capillary voltage of 3000V, and a fragmentor voltage of 100V. The molecular weight and repeating subunit analysis were conducted by deconvolving mass spectra from RPLC-MS total ion chromatograms with an open-source software iFAMS v.6.3 (iFAMS Quant), a Fourier-transform based algorithm developed by the Prell group to differentiate ion populations with high mass polydispersity (Figure S8, Supporting Information). 27-31

Method Validation: For specificity including forced degradation analysis, the HPMC-C₁₂ (0.06 mg/mL) and PEG-*b*-PLA NPs (0.1 mg/mL) were stressed under acidic (0.1 M HCl, 25 °C), basic (0.1 M NaOH, 25 °C), and heated (60 °C) conditions for ~20 hrs. The linearity was assessed over the range of $0.03-12~\mu g$ for HPMC-C₁₂, $0.01-5~\mu g$ for PEG-*b*-PLA, and 1-250~ng for Bimatoprost. The linearity range was defined based on the nominal hydrogel sample composition. Accuracy and precision of each analyte was assessed at 10%, 100%, and 120% level of the nominal sample loading. The average peak response and relative standard deviation (% RSD) were calculated for each analyte at each level (n=3). Signal to noise was assessed at a sample loading of 0.03 μg for HPMC-C₁₂, 0.01 μg for PEG-*b*-PLA, and 1 ng for Bimatoprost to determine the limit of quantitation (LOQ).

RESULTS AND DISCUSSION

Separation of Hydrogel Components by SEC and RPLC: The supramolecular PNP hydrogel contains components with vastly different molecular weights, conformation, and hydrophobicity (Scheme 1). The encapsulated cargo Bimatoprost is a small molecule (Log P = 3.2). HPMC-C₁₂ is a water soluble, hydrophilic polymer with hydrophobic modifiers. PEG-b-PLA is an amphiphilic block copolymer and can self-assemble to form nanoparticles by a nanoprecipitation process, driven by the hydrophobicity of PLA. The PEG-b-PLA NPs consist of PLA segments as core and PEG surface. We first focused on identifying a separation mode that could resolve and provide good recovery for all three components. Size based SEC, separation methods including hvdrodvnamic chromatography, and Field-Flow Fractionation are powerful in polymer and nanoparticle analysis. 32-35 SEC is widely applied for polymer characterization, which separates analytes based on their hydrodynamic radius, R_h. ³⁶ We assessed three SEC columns composed of hydrophilic polymer beads designed for the separation of high Mw water soluble polymers by connecting them to a CAD (Table S1, Supporting Information). Figure 1(a) displays a representative SEC-CAD chromatogram obtained using the TOSOH TSKgel G5000PWXL. A sufficient resolution could be achieved among the four pullulan sizing standards (1330 kDa to 0.99 kDa) in the Mw range of the hydrogel polymers. However, HPMC- C_{12} and PEG-b-PLA NPs showed co-elution in the SEC (Figure 1(a)). We investigated the co-elution by coupling SEC to MALS and an inline viscometer (IV) to determine Mw and R_h . The IV analysis revealed the HPMC- C_{12} and the PEG-b-PLA NPs had similar R_h (Table S2, Entry 1, 4, Supporting Information), which, combined with the apparent high dispersity of HPMC- C_{12} (peak width \sim 10 min at baseline), suggested the resolving power of SEC was insufficient for hydrogel composition analysis.

This SEC study also elucidated that the PEG-b-PLA polymer rapidly and spontaneously formed aggregates in the SEC condition and in organic/aqueous mixtures such as the HPLC diluent (Figure S1, Supporting Information). Before injection, when the PEG-b-PLA polymer was dissolved in 100% MeCN, no aggregates were detected by DLS (Figure S2 (a), Supporting Information). After injecting the polymer solution in SEC, the Mw increased from 22.5 kDa as a single polymer chain to ~11 MDa with a hydrodynamic radius of 15.5 nm, indicating the formation of nanosized aggregates (PEG-b-PLA Aggs) spontaneously in the SEC condition (Table S2, Entry 3, Supporting Information). The rapid aggregation of PEG-b-PLA polymers in an HPLC diluent was also detected by DLS (Diameter = 31 nm) upon adding water into the polymer/MeCN solution, which mimics the polymer aggregation during HPLC sample preparation (Figure S2 (a), Supporting Information). Due to the fast aggregation kinetics of the polymers in diluent or SEC condition, the PEG-b-PLA NPs or Aggs were injected as-is in the following studies without destabilizing with organic solvents. Also, the comparable R_h, chemical composition, and formation process of the PEG-b-PLA Aggs and the PEG-b-PLA NPs suggested that the Aggs can be used as the external standard to quantify NPs. In the following discussion, "PEG-b-PLA NPs" is used universally for both NPs and Aggs.

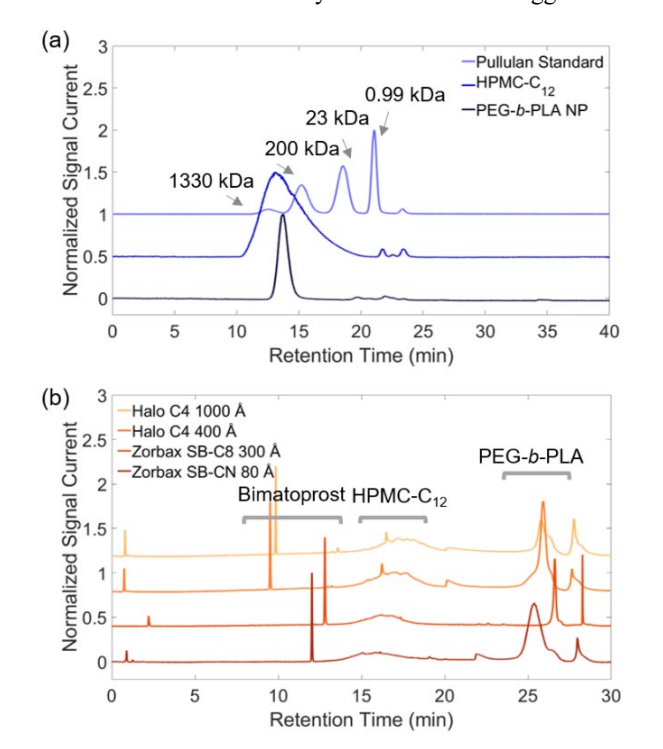


Figure 1. Representative chromatograms of Bimatoprost, HPMC-C₁₂, and PEG-*b*-PLA NPs using different separation principles: (a) SEC-CAD and (b) RPLC-CAD.

Since HPMC-C₁₂ and PEG-b-PLA NPs have similar sizes, reversed-phase (RP) separation was selected to leverage the analytes' hydrophobicity differences to achieve selectivity. Reversed-phase is a less common separation mode for nanoparticle characterization because the small pore size of the column packing materials may not allow good recovery. This was of particular concern since the PEG-b-PLA NPs would be injected as-is without dissociation into individual polymers in the diluent. To allow the elution of HPMC-C₁₂ and PEG-b-PLA, RP columns with 80-1000 Å pore sizes and less hydrophobic stationary phase chemistries were evaluated (Table S1, Supporting Information). Figure 1(b) shows a comparison of four RP columns using a generic linear gradient with a thermostat temperature of 30 °C. All RP columns resolved the 3 analytes. In the Zorbax SB-CN analysis (Figure 1(b), Table S3, Entry 1, Supporting Information), the PEG-b-PLA peak was broad, peakwidth at half-height = 0.90 min, likely due to restricted diffusion since the column is packed with fully porous particles (FPP) with a pore size of 80 Å. 37 The PEG-b-PLA peak became narrower by switching to a 300 Å C8 FPP column (Figure 1(b)). However, the retention/absorption of the HPMC-C₁₂ and PEG-b-PLA by the C8 stationary phase was strong and led to a low recovery for both polymers (Table S3, Entry 2, Supporting Information) and the sharp PEG-b-PLA peak was caused by only a small portion of analyte eluted. Halo C4 400 Å and 1000 Å columns packed with superficially porous particles (SPP) and less hydrophobic phases were tested to improve the mass transfer kinetics and recovery. Both C4 columns improved recovery of HPMC-C₁₂ and provided better resolution between Bimatoprost and HPMC-C₁₂ compared to SB-CN and SB-C8 columns, while producing reasonable peak shape and recovery for the PEG-b-PLA, especially the C4 400 Å column (Table S3, Entry 3-4, Supporting Information). While the C8 300 Å and C4 400 Å columns tested have similar pore sizes, they showed significant differences in recovery, indicating the stationary phase chemistry and particle technology played a key role in improving recovery. Therefore, the C4 SPP columns were pursued for further optimizations.

Elution Mechanism Discussion and Optimization: Due to the kinetically favored PEG-b-PLA aggregation in the sample diluent (25-50% MeCN in H₂O), the PEG-b-PLA was injected as-is in NP state (Figure S2(a), Supporting Information). The starting gradient of 5% MeCN, was not a thermodynamically good solvent for dissolving the NPs, so the injected NPs remained intact. When the pore size is much larger compared with the NPs size, the NPs could enter, precipitate and partition into the pores, operating in an interaction/adsorption mode. 38 When the pore size is similar to the NPs size, the NPs could be partially excluded from pore volume, operating with a hybrid mode of exclusion and interaction. As the gradient increased to ~95\% MeCN, the nanoparticles were destabilized on column and disrupted into individual PEG-b-PLA polymers (Figure S2 (b), Supporting Information). The high organic condition balanced out interactions between individual polymers and the stationary phases, thus the polymers moved quickly on the column and eluted. The on-column dissociation of NPs was confirmed by coupling RPLC with MALS detector, revealing the PEG-b-PLA peak Mw = 31 kDa (Figure S3, Supporting Information), corresponding to polymers instead of NPs (Mw = 11-23 MDa). This on-column dissociation-desorption-elution mechanism was likely responsible for the higher carryover observed in the 1000 Å column compared with the 400 Å (23.0% to 6.2%, respectively), due to the higher probability of NPs (diameter \sim 30 nm) partitioning into the 1000 Å pores, leading to slower dissociation of the NPs and desorption of the polymers, causing more carryover.

To further understand this phenomenon, we conducted a study to evaluate the effect of temperature and pore size on carryover (Table 1). Increasing temperature will accelerate mass transfer and absorption/desorption rates as a result of decreased mobile phase viscosity and increased analyte diffusivity. This led to reduced carryover at elevated temperature in both 1000 Å and 400 Å columns (< 2% above 50 °C). 38, 39 However, the temperature mainly accelerated the desorption-elution stage. The PEG-b-PLA did not fully elute if the mobile phase strength was reduced to lower organics (98% to 50%), while maintained at 60 °C (Figure S4, Supporting Information). The high organics eluent was critical to dissociate the NPs and a higher temperature facilitated the desorption and elution of the polymers to reduce carryover. Considering the 400 Å column has a lower likelihood of NPs partitioning into the pores compared with the 1000 Å, the 400 Å column was selected in the final method.

Table 1. Effect of Separation Temperature on the Carryover% of PEG-b-PLA.

Pore Size	Carryover (% Area/Area) ^a				
	30 °C	40 °C	50 °C	60 °C	
1000 Å	23.0%	7.2%	<2%	<2%	
400 Å	6.2%	6.4%	<2%	<2%	

^a Carryover% was determined by the ratio of the PEG-*b*-PLA peak area in the subsequent blank injection and the preceding PEG-*b*-PLA standard injection.

To improve the peak shape and height for HPMC-C₁₂, the thermostat temperature was raised to 50 °C. However, the peak shape was not significantly improved, and we instead observed an increase in retention (Figure S5(a)-(b), Supporting Information). This can be explained by the temperature dependent gelation of HPMC. As temperature increases, HPMC starts to lose its water shell, accompanied by an increase in polymer-polymer or polymer-stationary phase interactions. 40,41 A previous study reported gelation started at ~26 °C, but the onset temperature can vary depending on the composition and functionalization of HPMC. 41 To mitigate the impact of oncolumn gelation on the separation, while maintaining good recovery for PEG-b-PLA at 50-60 °C, an eluent step-gradient was implemented to elute the HPMC-C₁₂ and improve its oncolumn solubility (~80% MeCN) (Figure S5(c), Supporting Information). The sharpened HPMC-C₁₂ peak suggested the oncolumn absorption had been alleviated and resulted in a fast elution. The sensitivity of the HPMC-C₁₂ improved ~5 fold compared to the initial gradient program.

Diluent Study: To enable quantitative analysis of the intact PNP-2-10 hydrogel by RPLC-CAD, various diluents and sample extraction protocols were adapted to the hydrogel analysis and their extraction efficiency were compared. Extraction efficiency was determined by the ratio of the calculated amount of polymer from the RPLC-CAD calibration curve to the theoretical amount of polymer in the intact PNP-2-10 hydrogel. Both a 1-step dilution (gel dissolved as-is in the diluent) and a 2-step dilution (gel dissolved in the organic

portion first, followed by the aqueous portion) were assessed (Figure 2). Organic solvent was essential to effectively disrupt the hydrophobic interactions between HPMC-C₁₂ and PEG-b-PLA NPs. In an aqueous-only diluent, the extraction efficiency for both HPMC-C₁₂ and PEG-b-PLA NPs was lower than 30%. The 1-step and 2-step dilution were performed with MeCN/H₂O (25%/75%, v/v) instead of MeCN/H₂O (50%/50%, v/v) due to the peak splitting observed for Bimatoprost with the latter diluent. The 1-step dilution showed more variation between duplicate preparations (data not shown). In contrast to 100% MeCN (1st extraction solvent in the 2-step dilution), the reduced solvent strength of the 1-step dilution (25%/75% MeCN/H₂O) could not effectively disrupt the hydrophobic interactions between the PEG-b-PLA NPs and HPMC-C₁₂ nor fully solvate the NPs, leading to insufficient extraction and more variation in the quantitation. Two other solvents THF/H₂O (50%/50%, v/v) and DMSO/H₂O (50%/50%, v/v) were assessed in the 2-step preparation procedure, considering THF and DMSO have good solubility for the PEG-b-PLA NPs. However, DMSO/H2O showed poor extraction for both components. Although THF/H₂O showed better extraction compared to DMSO/H₂O, ultimately, the 2-step diluent MeCN/H₂O (25%/75%) was selected for the final procedure based on (1) better extraction efficiency for both polymeric components, achieving 90-110% of theoretical value in the PNP-2-10 hydrogel (Figure 2); and (2) reduced solvent incompatibility that caused peak splitting for hydrophilic cargo Bimatoprost.

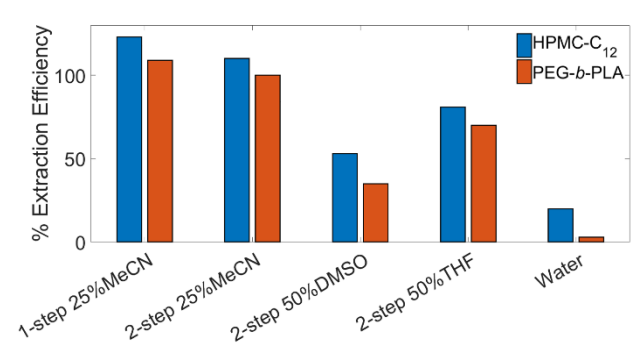


Figure 2. Extraction efficiency% of HPMC- C_{12} and PEG-b-PLA NPs (n=2) from the intact PNP-2-10 hydrogel with various diluents and sample extraction protocols.

Method Performance: The final RPLC-CAD method temperature was set at 60 °C to reduce carryover for PEG-b-PLA with the step-gradient for improved HPMC-C₁₂ peak shape. The method performance was validated for specificity, linearity, precision, accuracy, and LOQ following ICH Q2 guidance (Figure 3). Method specificity was demonstrated by no interference in the diluent blank affecting the quantitation of PNP-2-10 hydrogel (Figure 3(a)), as well as a forced degradation study by treating the mixture of HPMC-C₁₂ and PEG-b-PLA NPs with acid (0.1 M HCl), base (0.1 M NaOH), or heat (60 °C) stressed conditions for ~20 hr (Figure 3(b)). Following stressed conditions, a common degradant was observed eluting at ~6 min (before the HPMC-C₁₂). The degradant was formed most rapidly in the base stressed condition, accompanied by a loss of the PEG-b-PLA peak, likely associating it with the remaining PEG blocks after PLA blocks hydrolyzed (See **Polymer** Degradant Characterization by RPLC-MS Section). The method precision was determined by the %RSD of three replicate injections at 10%, 100% and 120% of the nominal sample loading. Each set of replicates have a %RSD lower than 3.0%, suggesting excellent method precision (Figure 3(c)). The accuracy of the method was within 90-110% (Figure 3(c), grey band) for all components at 10, 100, and 120% of the nominal loading level. Finally, since one application of this CAD method was to study the *in vitro* release of the encapsulated cargo and matrix polymers, the method's working range was validated spanning three orders of magnitude for each component in the PNP-2-10 hydrogel and fit with a second order polynomial equation. The polynomial fit was used for calibration to improve method accuracy compared to a linear fit due to the short linear response range of CAD. Over the validated range for each analyte (specified in **Experimental Section**), the correlation coefficient was >0.9999 for all three

components (Figure 3(d)-(f)). The LOQ level was established at 0.03 μg for HPMC-C₁₂, 0.01 μg for PEG-*b*-PLA NPs, and 1 ng for Bimatoprost with sufficient sensitivity for *in vitro* release analysis.

The method can be generalized to hydrogels encapsulating other payload types, demonstrated by the separation of a model protein (BSA) from PEG-b-PLA and HPMC-C₁₂ (Figure S6, Supporting Information). Given the cargo Bimatoprost (LogP 3.2) represents the hydrophobicity of most small molecule therapeutics and the C4 column is developed for analytes such as proteins and antibodies, this RPLC method should be suitable for analyzing hydrogels encapsulating a variety of synthetic and biological molecules.

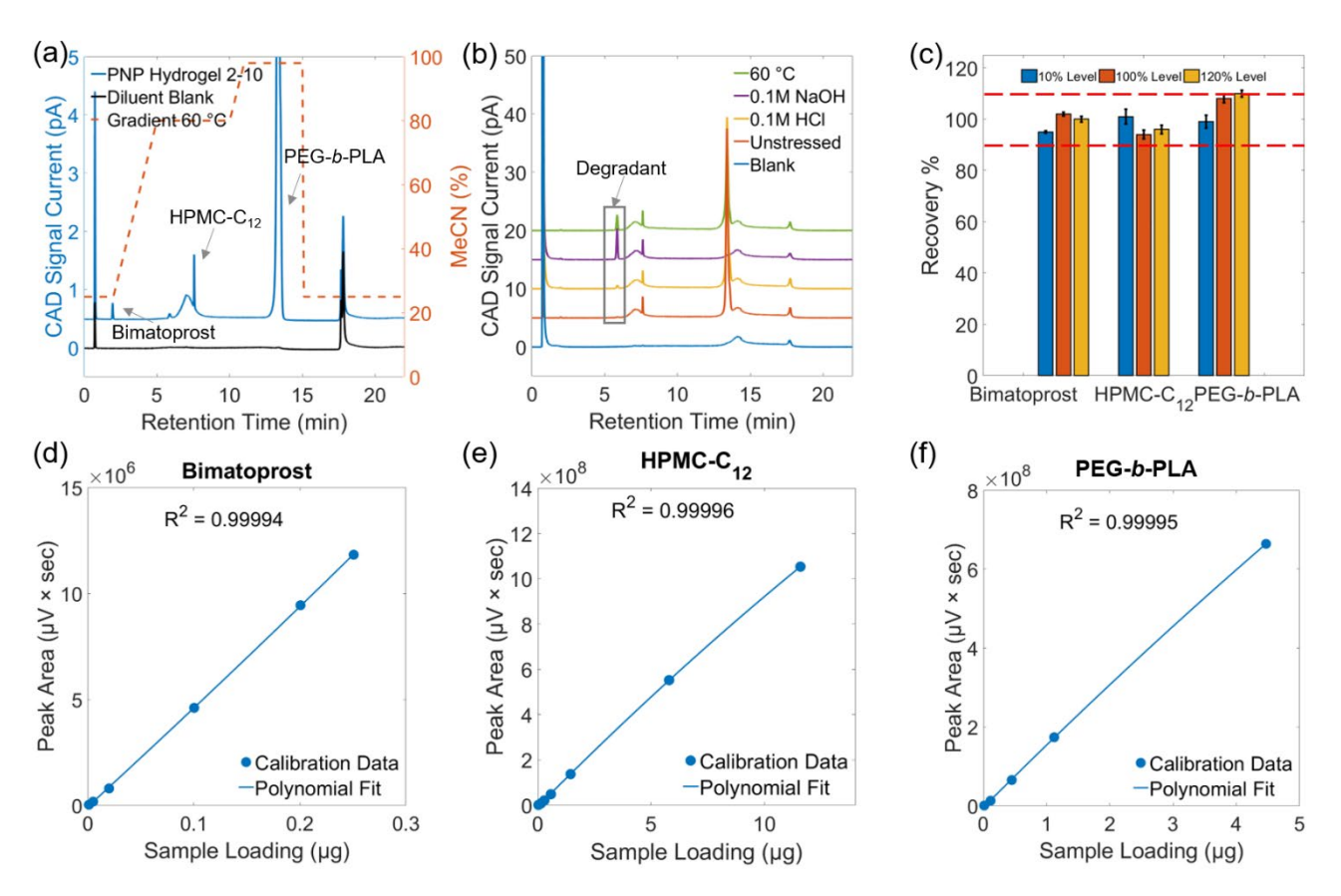


Figure 3. Final RPLC-CAD method chromatograms and performance. (a) RPLC-CAD chromatograms of the intact PNP-2-10 hydrogel (blue) and diluent blank (black), and final method gradient program (orange); (b) Forced degradation study of the HPMC-C₁₂ and PEG-*b*-PLA NPs; (c) Method accuracy (n=3) and precision assessment (n=3) at each concentration; Red line marked the target range of recovery%, 90-110%. Calibration data and polynomial fitting results of (d) Bimatoprost, (e) HPMC-C₁₂, and (f) PEG-*b*-PLA.

Application of RPLC-CAD and RPLC-MALS Method in Process Development: One application of this method was to monitor the concentrations of two polymeric components and Bimatoprost during an *in vitro* release study, which was included in our previous publication using a USP 7 dissolution apparatus. ²⁶ The RPLC-CAD method was applied here to evaluate the compatibility of E-beam sterilization with the hydrogel. E-beam sterilization is a common sterilization process for injectable formulations, involving continuous flow of high energy electrons into the treated materials. ⁴² However, E-beam may lead to polymer/cargo degradation and impact

rheological properties in the case of hydrogel formulations. PNP-2-10 hydrogels with and without E-beam treatment were assessed by the RPLC-CAD method. After E-beam treatment (dose range of 23-27 kGy), the Bimatoprost was found to be degraded as evidenced by its earlier elution in the sterilized hydrogel, and its concentration was below the method's detection limit (1 ng) (Figure 4(a)-(b)). Also notably, the HPMC-C₁₂ peak apex eluting time shifted earlier from 6.97 min in the control gel to 6.78 min in the e-beam treated gel, signifying a loss of hydrophobicity and degradation of the polymer after sterilization (Figure 4(b)). To further probe the

degradation of the HPMC-C₁₂, the RPLC method was coupled to MALS detector for inline Mw analysis, which revealed that the HPMC-C₁₂ light scattering peak area reduced ~2 fold after e-beam sterilization (Figure S7, Supporting Information). Since the light scattering signal is proportional to Mw, with the analyte's mass concentration and dn/dc values remained the same, the MALS results suggested the HPMC-C₁₂ Mw reduced ~2 fold due to e-beam treatment. ⁴³ Such polymer degradation affected the rheological properties of the hydrogel. Oscillatory shear rheology showed altered viscoelastic properties for the hydrogel following E-beam treatment, consistent with the RPLC-CAD results suggesting gel component degradation. An amplitude sweep showed the E-beam treated hydrogel had a

lower yield stress of 200 Pa compared with the untreated hydrogel's 1500 Pa (Figure 4(c)). Both the angular frequency and the amplitude sweep showed the sterilized hydrogel had an order of magnitude lower moduli (Figure 4 (d) and (e)) and a G' G" crossover point at a lower strain (Figure 4(e)), indicating the hydrogel became less stiff after E-beam irradiation. This study demonstrated the RPLC-CAD method provided chemical stability information for the hydrogel and assessed the impact of manufacturing process on the product quality. Importantly, the RPLC-CAD method can establish structure-property relationships by capturing the chemical changes and connecting those changes with rheological or other mechanical properties of the hydrogels.

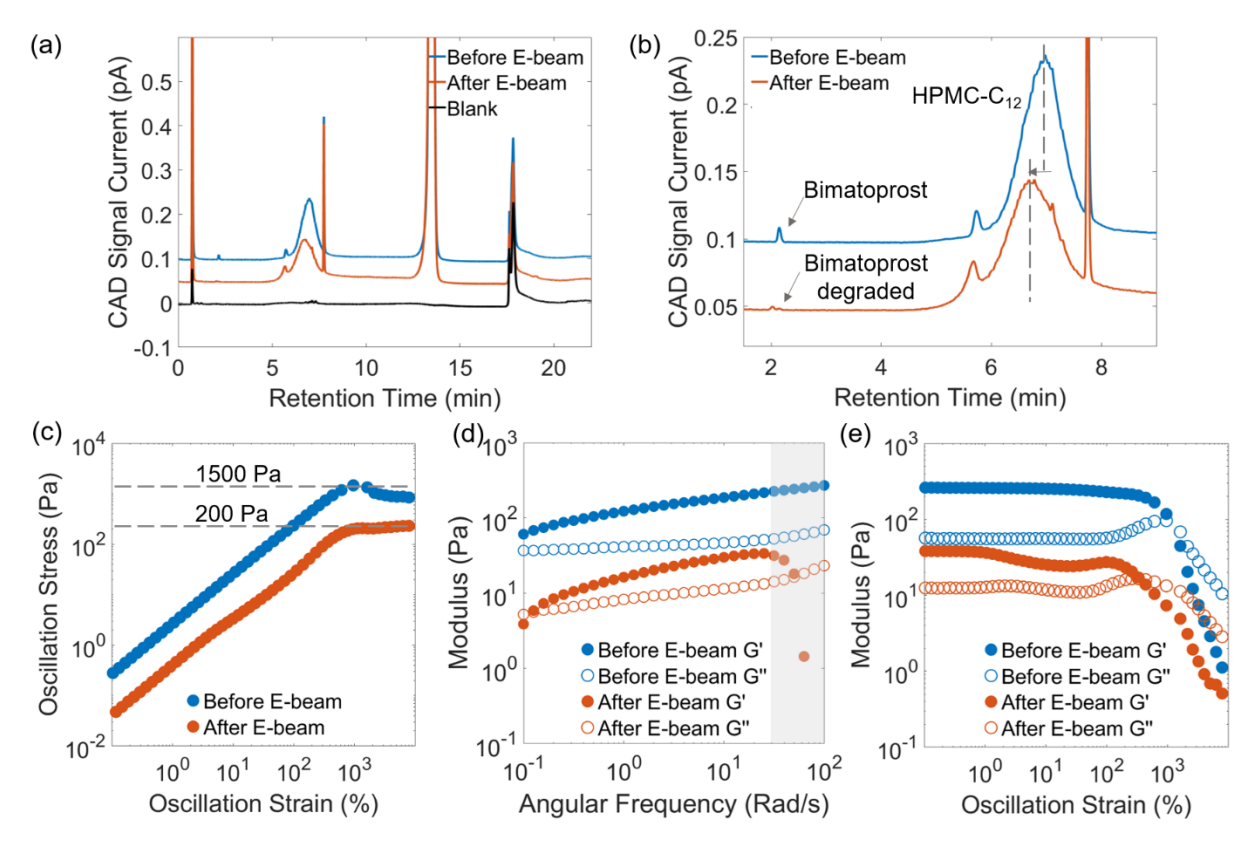


Figure 4. Characterization of hydrogels before and after E-beam sterilization. (a) Chemical composition analysis by the RPLC-CAD method; (b) Zoomed in chromatogram highlighted the degradation of Bimatoprost and the retention time shift of HPMC-C₁₂. (c) Strain-stress characterization; Moduli characterization by (d) frequency sweep and (e) amplitude sweep. The shaded data in (d) were instrument artifacts.

Polymer Degradant Characterization by RPLC-MS: As CAD and MS detectors both require volatile buffers as the mobile phase, the RPLC-CAD method was readily transferrable to an RPLC-MS system for higher resolution structural elucidation. Here, we probed the identity of the degradant observed in the earlier forced degradation study, particularly under the NaOH-stressed condition (Figure 3(b)). This degradant was also present at a low level in the intact hydrogel (Figure 3(a)). The mass spectrum of this degradant was collected in a qTOF mass spectrometer and processed using iFAMS. $^{27-31}$ In brief, polymer mass spectra consist of peak distributions with periodic spacing based on the mass of the repeated subunit and the polymer's net charge (Δ m/z), which can be separated by Fourier transform and normalized for

charge to yield much simpler mass reconstructions from multiply charged ion populations (Figure 5). The iFAMS deconvolution process, further detailed in Figure S8 (Supporting Information), revealed that the chromatographically-observed degradant is comprised solely of 4.5-6 kDa polymer with a repeated subunit of 44.05 Da, consistent with the 5 kDa PEG blocks used in the synthesis process for PEG-b-PLA copolymers. ²⁶

CONCLUSION

In summary, we presented a RPLC-CAD method as a label-free approach for characterizing CQAs of a supramolecular PNP hydrogel. A reversed phase C4 400Å SPP column provided the best specificity and recovery for hydrogel composition analysis. We found that the PEG-b-PLA NPs

PEG-b-PLA NaOH Degradant Mass Reconstruction

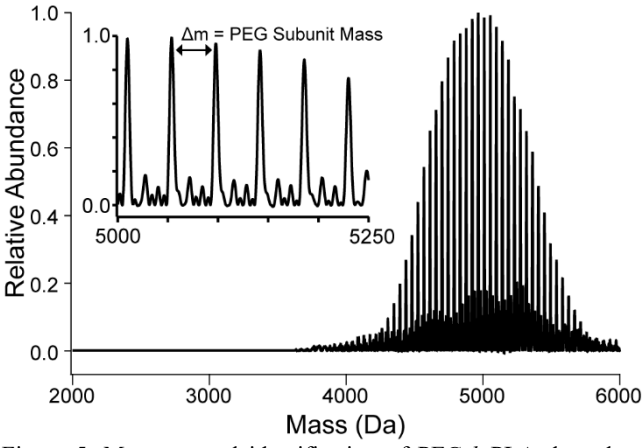


Figure 5. Mass spectral identification of PEG-b-PLA degradant peak from forced degradation study with NaOH. iFAMS mass reconstruction of the 6545XT qTOF polymer degradant spectrum, inset demonstrating identification of the repeated 44.05 Da PEG subunit.

adopted on-column dissociation-desorption-elution mechanism in the reversed phase condition, where high organics gradient was critical to disrupt the PEG-b-PLA NPs to PEG-b-PLA polymers, followed by desorption and elution. Coupling the RPLC method to a CAD detector, the active cargo as well as the polymeric components can be quantified simultaneously. The RPLC-CAD method was applied to characterize chemical changes of the hydrogels in forced degradation and E-beam studies, showing the method's capability to capture molecular level changes critical for the hydrogel material properties (i.e., rheological properties). In addition, the RPLC method is compatible with several hyphenations: (a) RPLC-MALS for inline molecular weight analysis, which was used to monitor polymer degradation and provide insights for the PEG-b-PLA NPs elution mechanism in the reversed phase condition, and (b) RPLC-MS for highresolution structural elucidation. With assistance from the iFAMS deconvolution algorithm, the repeating subunit and molecular weight of a polymer degradant were determined.

The PNP-2-10 supramolecular hydrogel was used as the model system in this study. Given the variety of stationary phase chemistries and particle technologies in RP columns and the universal detection of the CAD, it is possible to apply the RPLC-CAD methodology to characterize the CQAs of hydrogels with alternative cargos and gel chemistries. The RPLC-CAD approach is not necessarily limited to supramolecular hydrogels. In the case of chemically crossedlinked hydrogels, the released cargos and degraded/dissolved gel matrix can still be monitored in the release medium to study the gel degradation kinetics and structures. With suitable sample preparation/enrichment protocols, quantitation of gel polymers in vivo is feasible by the RPLC-CAD approach, which is useful for establishing IVIVC. Another implication of this study is to unlock a multi-attribute analysis workflow for hydrogels. Since MALS is a flow through and non-destructive detector, one- or two-dimensional hyphenation of RPLC-MALS with CAD can realize quantitation and Mw tracking in parallel. Overall, this analytical strategy enables the characterization of hydrogel compositions, release, and degradation, opening many opportunities such as establishing structure-property relationships in hydrogel design, IVIVC, quality control, and clinical translation of hydrogel therapeutics.

ASSOCIATED CONTENT

Supporting Information

Supporting Information including additional experimental details, MALS, DLS, iFAMS details, chromatograms, is available free of charge on the ACS Publications website.

AUTHOR INFORMATION

Corresponding Author

tang.shijia@gene.com eappel@stanford.edu

Author Contributions

S.T. and Z.P. contributed equally to this work

ACKNOWLEDGMENT

The authors acknowledged Peter Yehl, Karthik Nagapudi, Dennis Leung, Chris Crittenden, Jessie Ochoa, and Chloe Hu for their management, scientific support and expertise. E.L.M. was supported by the NIH Biotechnology Training Program (T32 GM008412). A.K.S. was supported by the National Science Foundation under award number CHE-1752994 to J.S.P. Scheme and TOC in this manuscript were created with BioRender.com

REFERENCES

- 1 Appel, E. A.; del Barrio, J.; Loh, X. J.; Scherman, O. A. Supramolecular polymeric hydrogels. *Chem. Soc. Rev.* **2012**, *41*, 6195-6214.
- 2 Guvendiren, M.; Lu, H. D.; Burdick, J. A. Shearthinning hydrogels for biomedical applications. *Soft Matter* **2012**, *8*, 260-272.
- 3 Li, J.; Mooney, D. J. Designing hydrogels for controlled drug delivery. *Nat. Rev. Mater.* **2016**. *1*, 1-17.
- 4 Rosales, A. M.; Anseth, K. S. The design of reversible hydrogels to capture extracellular matrix dynamics. *Nat. Rev. Mater.* **2016**, *1*, 1-15.
- 5 Tong, X.; Yang, F. Recent Progress in Developing Injectable Matrices for Enhancing Cell Delivery and Tissue Regeneration. *Adv. Healthc. Mater.* **2018**, *7*, e1701065.
- 6 Uman, S.; Dhand, A.; Burdick, J. A. Recent advances in shear-thinning and self-healing hydrogels for biomedical applications. *J. Appl. Polym. Sci.* **2020**, *137*, 48668.
- 7 Correa, S.; Grosskopf, A. K.; Lopez Hernandez, H.; Chan, D.; Yu, A. C.; Stapleton, L. M.; Appel, E. A. Translational Applications of Hydrogels. *Chem. Rev.* **2021**, *121*, 11385-11457.
- 8 Mann, J. L.; Yu, A. C.; Agmon, G.; Appel, E. A. Supramolecular polymeric biomaterials. *Biomater. Sci.* **2017**, *6*, 10-37.
- 9 Mandal, A.; Clegg, J. R.; Anselmo, A. C.; Mitragotri, S. Hydrogels in the clinic. *Bioeng. Transl. Med.* **2020**, *5*, e10158. 10 Omar, J.; Ponsford, D.; Dreiss, C. A.; Lee, T. C.; Loh,
- X. J. Supramolecular Hydrogels: Design Strategies and Contemporary Biomedical Applications. *Chem. Asian J.* **2022**, *17*, e202200081.
- 11 Wei, L.; Chen, J.; Zhao, S.; Ding, J.; Chen, X. Thermosensitive polypeptide hydrogel for locally sequential delivery of two-pronged antitumor drugs. *Acta Biomater.* **2017**, *58*, 44-53.
- 12 Hu, C.; Zhang, F.; Long, L.; Kong, Q.; Luo, R.; Wang, Y. Dual-responsive injectable hydrogels encapsulating drug-

- loaded micelles for on-demand antimicrobial activity and accelerated wound healing. *J. Control Release* **2020**, *324*, 204-217.
- 13 Chen, K.; Wu, Z.; Liu, Y.; Yuan, Y.; Liu, C. Injectable Double-Crosslinked Adhesive Hydrogels with High Mechanical Resilience and Effective Energy Dissipation for Joint Wound Treatment. *Adv. Funct. Mater.* **2021**, *32*, 2109687.
- 14 Artzi, N.; Oliva, N.; Puron, C.; Shitreet, S.; Artzi, S.; bon Ramos, A.; Groothuis, A.; Sahagian, G.; Edelman, E. R. In vivo and in vitro tracking of erosion in biodegradable materials using non-invasive fluorescence imaging. *Nat. Mater.* **2011**, *10*, 704-709.
- Lai, C. Y.; Wu, P. J.; Roffler, S. R.; Lee, S. T.; Hwang, S. M.; Wang, S. S.; Wang, K.; Hsieh, P. C. Clearance kinetics of biomaterials affects stem cell retention and therapeutic efficacy. *Biomacromolecules* **2014**, *15*, 564-573.
- 16 Segovia, N.; Pont, M.; Oliva, N.; Ramos, V.; Borros, S.; Artzi, N. Hydrogel doped with nanoparticles for local sustained release of siRNA in breast cancer. *Adv. Healthc. Mater.* **2015**, *4*, 271-280.
- 17 Ma, X.; Sun, X.; Hargrove, D.; Chen, J.; Song, D.; Dong, Q.; Lu, X.; Fan, T. H.; Fu, Y.; Lei, Y. A Biocompatible and Biodegradable Protein Hydrogel with Green and Red Autofluorescence: Preparation, Characterization and In Vivo Biodegradation Tracking and Modeling. *Sci. Rep.* **2016**, *6*, 19370. 18 Liu, C.; Bae, K. H.; Yamashita, A.; Chung, J. E.; Kurisawa, M. Thiol-Mediated Synthesis of Hyaluronic Acid-Epigallocatechin-3-O-Gallate Conjugates for the Formation of Injectable Hydrogels with Free Radical Scavenging Property and Degradation Resistance. *Biomacromolecules* **2017**, *18*, 3143-
- 19 Kivijarvi, T.; Oyvind, G.; Yassin, M. A.; Jain, S.; Yamada, S.; Morales-Lopez, A.; Mustafa, K.; Finne-Wistrand, A. Hybrid material based on hyaluronan hydrogels and poly(l-lactide-co-1,3-trimethylene carbonate) scaffolds toward a cell-instructive microenvironment with long-term in vivo degradability. *Mater. Today Bio.* **2022**, *17*, 100483.

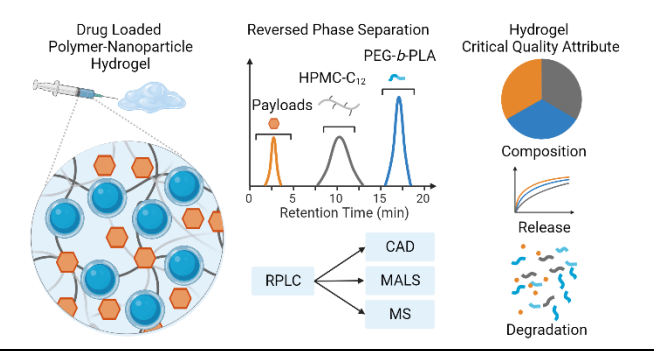
3155.

- 20 Liang, Y.; Hao, Y.; Wu, Y.; Zhou, Z.; Li, J.; Sun, X.; Liu, Y. N. Integrated Hydrogel Platform for Programmed Antitumor Therapy Based on Near Infrared-Triggered Hyperthermia and Vascular Disruption. *ACS Appl. Mater. Interfaces* **2019**, *11*, 21381-21390.
- Appel, E. A.; Tibbitt, M. W.; Webber, M. J.; Mattix, B. A.; Veiseh, O.; Langer, R. Self-assembled hydrogels utilizing polymer-nanoparticle interactions. *Nat. Commun.* **2015**, *6*, 6295.
- Stapleton, L. M.; Steele, A. N.; Wang, H.; Lopez Hernandez, H.; Yu, A. C.; Paulsen, M. J.; Smith, A. A. A.; Roth, G. A.; Thakore, A. D.; Lucian, H. J.; et al. Use of a supramolecular polymeric hydrogel as an effective post-operative pericardial adhesion barrier. *Nat. Biomed. Eng.* **2019**, *3*, 611-620.
- 23 Roth, G. A.; Gale, E. C.; Alcantara-Hernandez, M.; Luo, W.; Axpe, E.; Verma, R.; Yin, Q.; Yu, A. C.; Hernandez, H. L.; Maikawa, C. L.; et al. Injectable Hydrogels for Sustained Codelivery of Subunit Vaccines Enhance Humoral Immunity. *ACS Cent. Sci.* **2020**, *6*, 1800-1812.
- Yu, A. C.; Lian, H.; Kong, X.; Lopez Hernandez, H.; Qin, J.; Appel, E. A. Physical networks from entropy-driven non-covalent interactions. *Nat. Commun.* **2021**, *12*, 746.
- 25 Grosskopf, A. K.; Labanieh, L.; Klysz, D. D.; Roth, G. A.; Xu, P.; Adebowale, O.; Gale, E. C.; Jons, C. K.; Klich, J. H.; Yan, J. Delivery of CAR-T cells in a transient injectable stimulatory hydrogel niche improves treatment of solid tumors. *Sci. Adv.* **2022**, *8*, eabn8264.
- Meany, E. L.; Andaya, R.; Tang, S.; Kasse, C. M.; Fuji, R. N.; Grosskopf, A. K.; d'Aquino, A. L.; Bartoe, J. T.; Ybarra, R.; Shelton, A.; et al. Injectable Polymer-Nanoparticle Hydrogel

- for the Sustained Intravitreal Delivery of Bimatoprost. *Adv. Therap.* **2022**, *6*, 2200207.
- 27 Cleary, S. P.; Thompson, A. M.; Prell, J. S. Fourier Analysis Method for Analyzing Highly Congested Mass Spectra of Ion Populations with Repeated Subunits. *Anal. Chem.* **2016**, *88*, 6205-6213.
- 28 Cleary, S. P.; Li, H.; Bagal, D.; Loo, J. A.; Campuzano, I. D. G.; Prell, J. S. Extracting Charge and Mass Information from Highly Congested Mass Spectra Using Fourier-Domain Harmonics. *J. Am. Soc. Mass Spectrom.* **2018**, *29*, 2067-2080.
- 29 Cleary, S. P.; Prell, J. S. Liberating Native Mass Spectrometry from Dependence on Volatile Salt Buffers by Use of Gabor Transform. *ChemPhysChem* **2019**, *20*, 519-523.
- Rolland, A. D.; Prell, J. S. Approaches to Heterogeneity in Native Mass Spectrometry. *Chem. Rev.* **2022**, *122*, 7909-7951.
- 31 Swansiger, A. K.; Marty, M. T.; Prell, J. S. Fourier-Transform Approach for Reconstructing Macromolecular Mass Defect Profiles. *J. Am. Soc. Mass Spectrom.* **2022**, *33*, 172-180.
- 32 Pirok, B. W. J.; Abdulhussain, N.; Aalbers, T.; Wouters, B.; Peters, R. A. H.; Schoenmakers, P. J. Nanoparticle Analysis by Online Comprehensive Two-Dimensional Liquid Chromatography combining Hydrodynamic Chromatography and Size-Exclusion Chromatography with Intermediate Sample Transformation. *Anal. Chem.* **2017**, *89*, 9167-9174.
- 33 Edam, R.; Eeltink, S.; Vanhoutte, D. J.; Kok, W. T.; Schoenmakers, P. J. Hydrodynamic chromatography of macromolecules using polymer monolithic columns. *J. Chrom. A* **2011**, *1218*, 8638-8645.
- 34 Li, Y.; Shen, H.; Lyons, J. W.; Sammler, R. L.; Brackhagen, M.; Meunier, D. M. Size-exclusion chromatography of ultrahigh molecular weight methylcellulose ethers and hydroxypropyl methylcellulose ethers for reliable molecular weight distribution characterization. *Carbohydr. Polym.* **2016**, *138*, 290-300.
- 35 Engel, A.; Ploger, M.; Mulac, D.; Langer, K. Asymmetric flow field-flow fractionation (AF4) for the quantification of nanoparticle release from tablets during dissolution testing. *Int. J. Pharm.* **2014**, *461*, 137-144.
- 36 Striegel, A. M. Modern size-exclusion liquid chromatography: practice of gel permeation and gel filtration chromatography; Wiley, 2009.
- 37 Wagner, B. M.; Schuster, S. A.; Boyes, B. E.; Shields, T. J.; Miles, W. L.; Haynes, M. J.; Moran, R. E.; Kirkland, J. J.; Schure, M. R. Superficially porous particles with 1000A pores for large biomolecule high performance liquid chromatography and polymer size exclusion chromatography. *J. Chrom. A* **2017**, *1489*, 75-85.
- 38 Uliyanchenko, E.; van der Wal, S.; Schoenmakers, P. J. Challenges in polymer analysis by liquid chromatography. *Polym. Chem.* **2012**, *3*, 2313-2335.
- 39 Antia, F. D.; Horvath, C. High-Performance Liquid Chromatography at Elevanted Temperatures: Examination of Conditions for the Separation of Large Molecules. *J. Chrom.* **1988**, *435*, 1-15.
- 40 Sarkar, N. Thermal gelation properties of methyl and hydroxypropyl methylcellulose. *J. Appl. Polym. Sci.* **1979**, *24*, 1073-1087.
- 41 Greiderer, A.; Steeneken, L.; Aalbers, T.; Vivo-Truyols, G.; Schoenmakers, P. Characterization of hydroxypropylmethylcellulose (HPMC) using comprehensive two-dimensional liquid chromatography. *J. Chrom. A* **2011**, *1218*, 5787-5793.
- 42 Tohfafarosh, M.; Baykal, D.; Kiel, J. W.; Mansmann, K.; Kurtz, S. M. Effects of gamma and e-beam sterilization on the chemical, mechanical and tribological properties of a novel hydrogel. *J. Mech. Behav. Biomed. Mater.* **2016**, *53*, 250-256.

Authors are required to submit a graphic entry for the Table of Contents (TOC) that, in conjunction with the manuscript title, should give the reader a representative idea of one of the following: A key structure, reaction, equation, concept, or theorem, etc., that is discussed in the manuscript. Consult the journal's Instructions for Authors for TOC graphic specifications.

Insert Table of Contents artwork here



Supporting Information

Label-Free Composition Analysis of Supramolecular Polymer – Nanoparticle Hydrogels by Reversed-Phase Liquid Chromatography Coupled with a Charged Aerosol Detector

Shijia Tang ^{a,#,*}, Zachary Pederson ^{a,#}, Emily L. Meany ^b, Chun-Wan Yen ^a, Andrew K. Swansiger ^e, James S. Prell ^e, Bifan Chen ^a, Abigail K. Grosskopf ^f, Noah Eckman ^c, Grace Jiang ^b, Julie Baillet ^d, Jackson D. Pellett ^a, Eric A. Appel ^{b,*}

Corresponding author: tang.shijia@gene.com, eappel@stanford.edu

Table of Content

Table S1	S4
Table S2	S5
Figure S1	S6
Figure S2	S6
Table S3	
Figure S3	S8
Figure S4	
Figure S5	
Figure S6	S11
Figure S7	S12
Figure S8	S13

^a Small Molecule Pharmaceutical Sciences, Genentech, Inc., South San Francisco, CA 94080, USA

^b Department of Bioengineering, Stanford University, Stanford, CA 94305, USA.

^c Department of Chemical Engineering, Stanford University, Stanford, CA 94305, USA.

^d Department of Materials Science and Engineering, Stanford University, Stanford, CA 94305, USA.

^e Department of Chemistry and Biochemistry, University of Oregon, Eugene, Oregon 97403-1253, USA

^f Preclinical and Translational Pharmacokinetics and Pharmacodynamics, Genentech, Inc., South San Francisco, CA 94080, USA

[#]These authors contributed equally to this work

Experimental Conditions:

Unless otherwise stated, all methods and conditions were the same as indicated in the main text.

1. Synthesis of Polymers, Polymer Nanoparticles, and Hydrogels:

Synthesis of HPMC-C₁₂ and PEG-b-PLA

HPMC-C₁₂ and PEG-*b*-PLA were prepared and purified according to previously reported procedures. ¹ The HPMC-C₁₂ molecular weight (Mw) was determined by size exclusion chromatography coupled to multi-angle light scattering (see instrument sections below for details), Mw = 372 kDa (PDI=1.2). PEG-*b*-PLA molecular weight was determined by Gel Permeation Chromatography (GPC) with DMF as eluent Mw= 22.5 kDa (PDI=1.07). The PEG block was 5 kDa and PLA block was 18 kDa determined by NMR.

Preparation of PEG-b-PLA Nanoparticles

PEG-b-PLA nanoparticles (NPs) were prepared by a nanoprecipitation process and analyzed as previously reported. ¹ In brief, the nanoprecipitation process started by adding 1 mL solution of PEG-b-PLA (50 mg/mL in 1/3 DMSO/Acetonitrile (v/v)) dropwise into 10 mL water under stirring (stir rate 600 rpm). Then, the NPs were purified by ultracentrifugation using Millipore Amicon Ultra-15 filter (molecular weight cutoff 10 kDa; EMD Millipore, Burlington, MA). The purified NPs were re-suspended in Phosphate-Buffered Saline (PBS) to reach final concentration of 200 mg/mL (20 wt%). NPs size and dispersity were characterized by dynamic light scattering (DLS, Wyatt Technology, Santa Barbara, CA) (diameter = 31.8 nm, PDI = 0.04).

2. Instruments and Chromatographic Conditions:

SEC-CAD Analysis

SEC separation was carried out using an Acclaim SEC-1000 7.8 × 300 mm (Thermo Fisher Scientific, Waltham, MA), a PolySep GFC-P 6000 7.8 × 300 mm (Phenomenex, Torrance, CA), or a TSKgel G5000PWXL 7.8 × 300 mm (TOSOH Bioscience, King of Prussia, PA). Mobile phase was 80% 20 mM ammonium acetate/20% MeCN (v/v) with a flow rate of 0.5-1.0 mL/min. 10%-20% MeCN was added to suppress the secondary interaction between the column phases and the polymers. ² The thermostat temperature was 30 °C. The chromatography data was processed and analyzed in Empower (Waters, Milford, MA).

SEC-MALS Analysis

The SEC-MALS-IV-dRI analysis used an Agilent 1260 series HPLC (Agilent Technologies, Santa Clara, CA) equipped with a quaternary pump, vacuum degasser, temperature controlled autosampler, thermostatted column compartment, and a diode array detector. The instrument was further coupled to the multi-angle light scattering (MALS) detector DAWN (8 or 18 angle detector), inline viscometer (IV) Viscostar DAWN, and a differential refractometer (dRI) Optilab (Wyatt Technology, Santa Barbara, CA) for molecular weight (Mw) and hydrodynamic radius (Rh) analysis. A TSKgel G5000PWXL 7.8×300 mm (TOSOH Bioscience, King of Prussia, PA)

SEC column was used. The method mobile phase was 10 mM Potassium Phosphate (pH = 7)/Acetonitrile (80/20, v/v) with a flow rate of 0.5-1 mL/min. The thermostat temperature was 30 °C. The chromatography data was processed and analyzed in Astra 7 or 8 (Wyatt Technology, Santa Barbara, CA). The dn/dc value used for HPMC- C_{12} molecular weight analysis was 0.14 g/mL. ³ The dn/dc value used for PEG-*b*-PLA NPs analysis was 0.043 g/mL, estimated based on the weighted average of the individual polymer block dn/dc values: PEG 0.13 g/mL and PLA 0.019 g/mL. ^{4,5}

RPLC-CAD Column Screening

RPLC separation was carried out on the following columns: Zorbax SB-CN 80 Å 3.0 × 100 mm (Agilent, Santa Clara, CA), Zorbax SB-C8 300 Å 3.0 × 150 mm (Agilent, Santa Clara, CA), Halo C4 400 Å 2.1 × 150 mm (Advanced Materials Technology, Wilmington, DE), and Halo C4 1000 Å 2.1 × 150 mm 1000 Å (Advanced Materials Technology, Wilmington, DE). Mobile phase A (MPA) was 0.05% (v/v) TFA in water and mobile phase B (MPB) was MeCN. A generic gradient was used to evaluate those columns starting at 5%MPB for 1 min, then ramping to 95%MPB over 23 mins, maintaining 95% MPB for 1 min before bringing it back to the original gradient condition. The total method run time was 30 mins. Flow rate was 0.5 mL/min for columns with 2.1 mm internal diameter (ID) and 0.8 mL/min for columns with 3.0 mm ID. Thermostat temperature was set at 30 °C unless otherwise specified.

RPLC-MALS Analysis

The RPLC-MALS-dRI analysis used an Agilent 1260 series HPLC (Agilent Technologies, Santa Clara, CA) equipped with a quaternary pump, vacuum degasser, temperature controlled autosampler, thermostatted column compartment, and a diode array detector. The instrument was further coupled to the multi-angle light scattering (MALS) detector DAWN (8 or 18 angle detector), and a differential refractometer (dRI) Optilab (Wyatt Technology, Santa Barbara, CA) for molecular weight (Mw) analysis. The method gradient used the same final method step gradient as described in the main text. Baseline was subtracted to account for the refractive index changes due to gradient elution. The chromatography data was processed and analyzed in Astra 7 or 8 (Wyatt Technology, Santa Barbara, CA). The dn/dc value used for molecular weight analysis was 0.0497 g/mL for PEG-b-PLA. This value was determined from the dRI signal with a known injection amount and the assumption of 100% mass recovery.

Dynamic Light Scattering (DLS)

Unless otherwise stated, benchtop DLS analysis was conducted by Zetasizer Ultra (Malvern, UK). PEG-b-PLA NPs were prepared by nanoprecipitation as indicated above in the Preparation of PEG-b-PLA Nanoparticles Experimental Section. The NPs were diluted 100 folds in 100% water, 25% MeCN/75% water (v/v), or 100% MeCN and the diluted samples were analyzed with Zetasizer. For polymer analysis, PEG-b-PLA polymers were dissolved in 100% MeCN at 2.5 mg/mL, and then diluted with appropriate amount of MeCN or H₂O to reach 0.5 mg/mL in 25%MeCN/75%H₂O (v/v), 50%MeCN/50%H₂O (v/v), or 100% MeCN and analyzed by the Zetasizer.

Rheology

Rheological characterization was performed on a TA Instruments DHR-2 stress-controlled rheometer (New Castle, Delaware). All experiments followed the protocol used in previous literature. ¹ In brief, a 20 mm diameter serrated plate geometry was used with a 500 µm gap. Temperature was maintained at 25 °C. A frequency of 10 rad/s was used for strain amplitude sweeps. A constant 1% strain was used for frequency sweep measurements in the linear viscoelastic regime.

Results:

1. Column Information

Table S1. SEC and RP Columns Used for HPMC-C₁₂ and PEG-b-PLA NP Analysis

Column Name	Separation Mode	Phases	Particle Size (µm)	Particle Technology	Pore Size (Å)
TSKgel G5000PWXL		Hydroxylated polymethacrylate	10		1000
Acclaim SEC-1000	SEC	Proprietary hydrophilic resin	7		1000
PolySep GFC-P 6000		Hydrophilic polymer	Not listed		Not listed
Zorbax SB-CN		Cyano groups	3.5	Fully porous	80
Zorbax SB-C8	RP	C8 groups	3.5	Fully porous	300
Halo 400Å C4	I RP	C4 groups	3.4	Superficially porous	400
Halo 1000Å C4		C4 groups	2.7	Superficially porous	1000

2. Polymer and Nanoparticle Characterization by SEC-MALS-IV-dRI

Table S2. Mw and Size Measurements by SEC-MALS-IV-dRI.

Entry	Materials	Self-Assembly Process	Mw (kDa)	PDI	R _{h,z} (nm)
1	HPMC-C ₁₂	Not applicable	372	1.2	34.8
2	PEG-b-PLA Agg	Dissolve polymer in MeCN and add water to reach final 25% MeCN/75% water then inject on SEC	12521	1.2	17.2
3	PEG-b-PLA Agg	Dissolve polymer in MeCN and inject on SEC	11447	1.0	15.5
4	PEG-b-PLA NP	Nanoprecipitation	23334	1.0	25.4

The Agg and NP were comparable in size and chemical identity and so NP are used in the following studies to refer both Agg and NP.

3. Self-Assembly of PEG-b-PLA Polymer

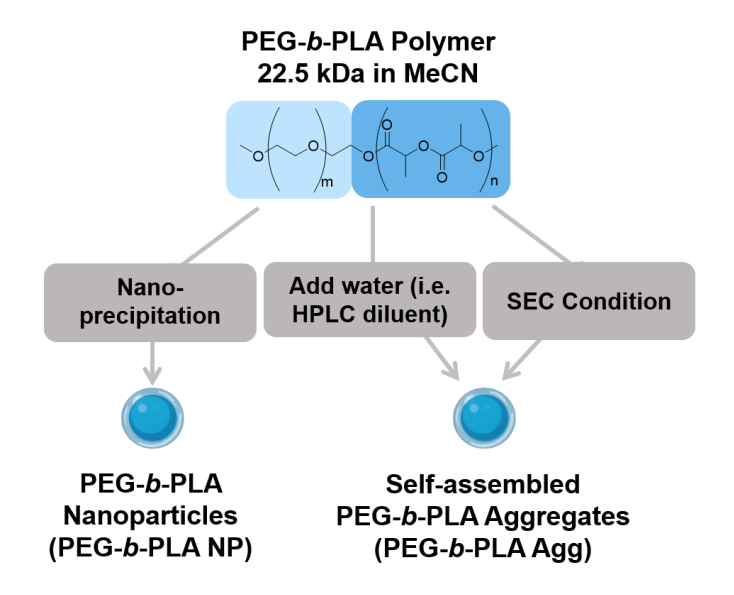


Figure S1. Illustration of PEG-*b*-PLA polymers and their formation of PEG-*b*-PLA nanoparticles or aggregates.

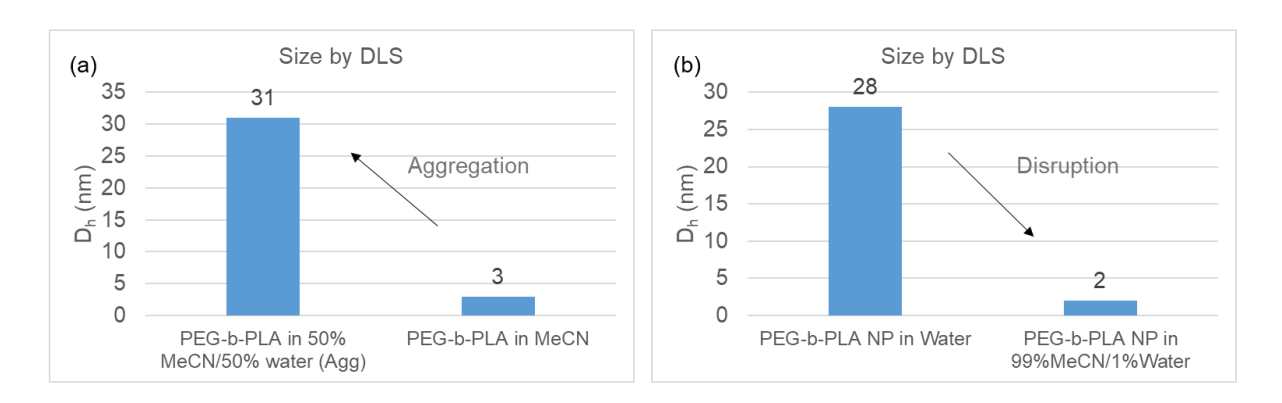


Figure S2. Size characterization of (a) PEG-*b*-PLA polymers and (b) PEG-*b*-PLA NPs in various diluents by dynamic light scattering.

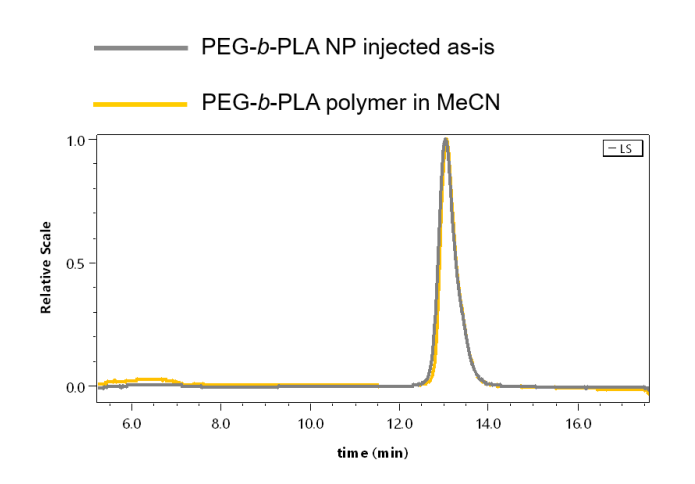
4. Reversed Phase Column Evaluation

Table S3. Relative Recovery Assessment in Reversed Phase Columns

Entry Column		Normalized Peak Area			Peak Width at Half-Height (min)	
		Bimatoprost	HPMC-C ₁₂	PEG-b-PLA	PEG-b-PLA	
1	SB-CN 80 Å	1.0	6.1	13.5	0.90	
2	SB-C8 300 Å	1.0	4.3	2.6	0.14	
3	C4 400 Å	1.0	9.5	11.4	0.36	
4	C4 1000 Å	1.0	8.6	5.9	0.47	

The column evaluation was conducted using a mixture of Bimatoprost, HPMC-C₁₂, PEG-*b*-PLA NPs spiked at a fixed ratio. To assess the relative recovery of HPMC-C₁₂ and PEG-*b*-PLA in different RP columns, the peak area of those polymers was normalized against the peak area of Bimatoprost analyzed using the same column. A lower value indicates a lower recovery for the analyte. Among the 4 columns, the C4 400 and 1000 Å columns demonstrated the highest relative recovery for the HPMC-C₁₂. The SB-CN 80 Å and C4 400 Å showed good recovery for PEG-*b*-PLA, however, the SB-CN showed poor peak shape/width for PEG-*b*-PLA, while in the C4 400 Å column, PEG-*b*-PLA peak width was significantly reduced.

5. RPLC-MALS for PEG-b-PLA Mw Analysis On-Column



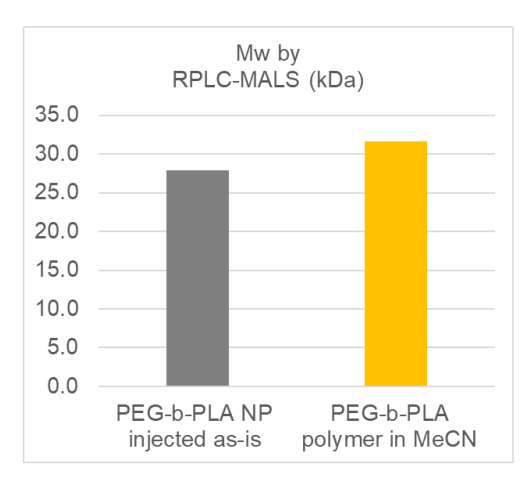


Figure S3. RPLC-MALS light scattering signal (left) and Mw analysis (right) of PEG-*b*-PLA NPs (grey) or polymers (yellow).

6. Effect of Isocratic Gradient on PEG-b-PLA Elution

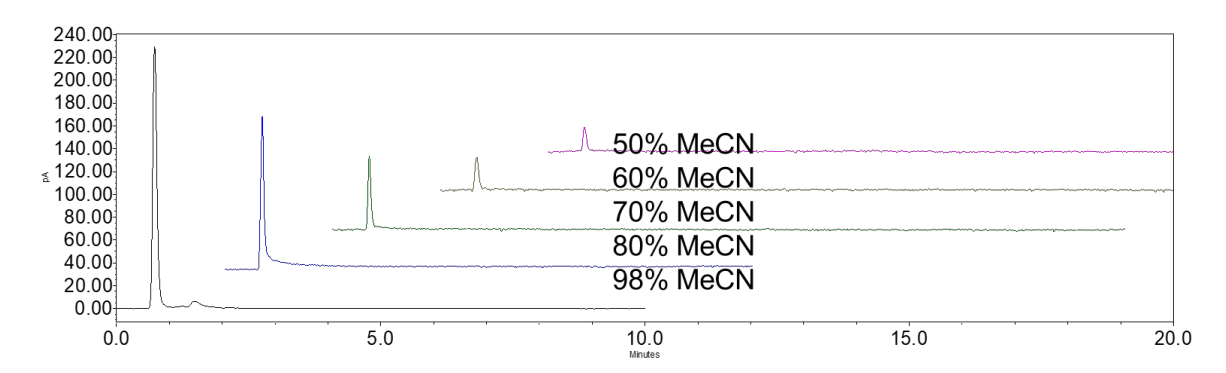


Figure S4. The RPLC-CAD analysis of PEG-*b*-PLA NPs using the 400 Å C4 column with various strength of isocratic eluent at 60 °C.

7. Improving HPMC-C₁₂ Peak Shape

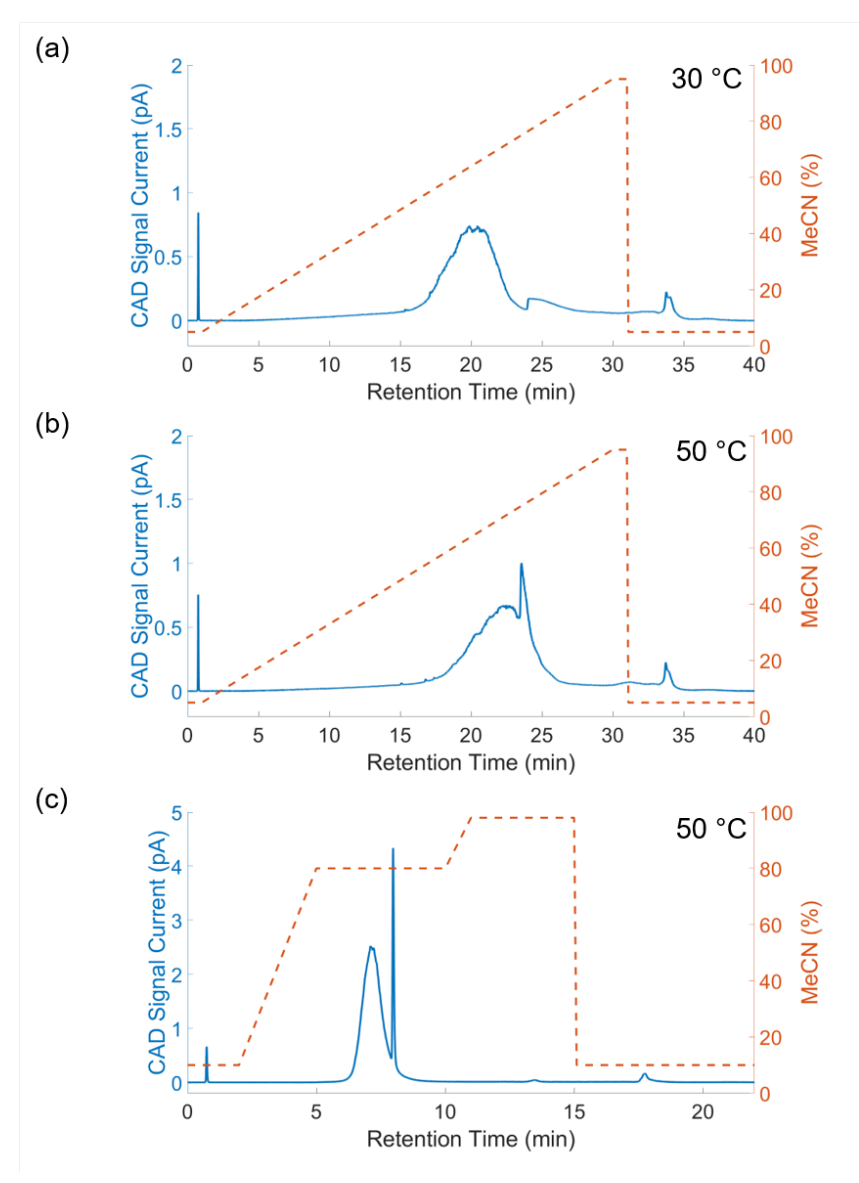


Figure S5. Method optimization study to improve HPMC- C_{12} peak shape with a linear gradient at (a) 30 °C, (b) 50 °C, and (c) a step gradient at 50 °C.

8. RPLC-CAD Method Suitability for Alternative Cargos

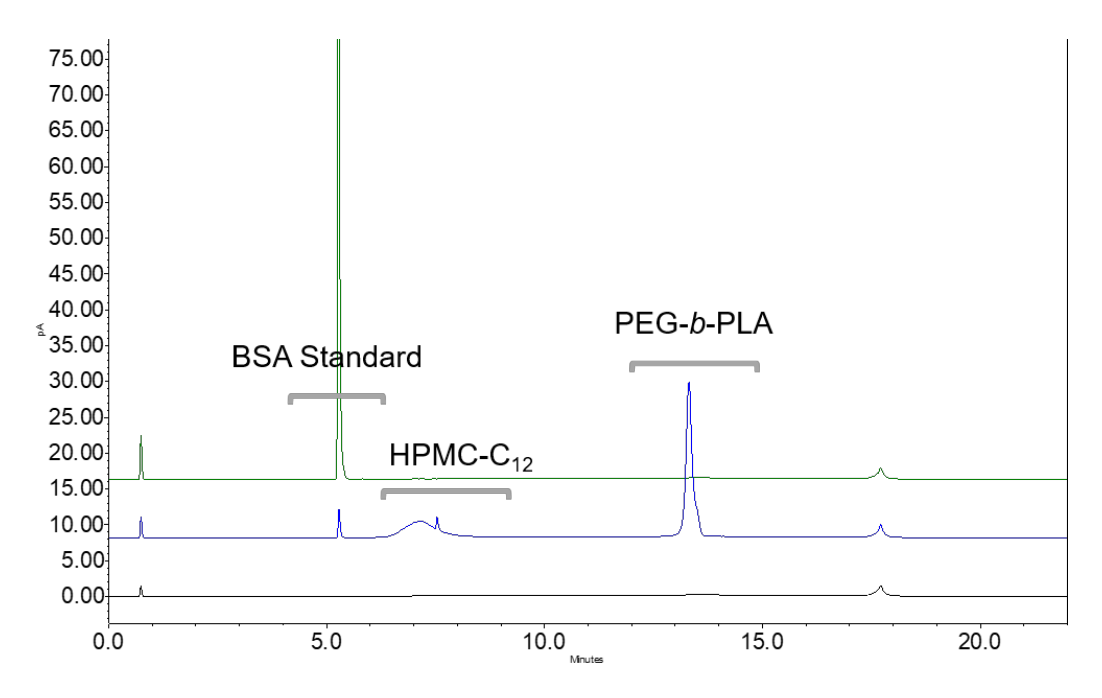


Figure S6. Method suitability study demonstrated by the overlay of diluent blank (black), BSA standard (green), and a mixture of BSA, HPMC- C_{12} and PEG-b-PLA NPs (blue), supporting the applicability of this method to alternative cargos such as proteins.

9. Analysis of HPMC-C₁₂ Before and After E-beam Sterilization by RPLC-MALS

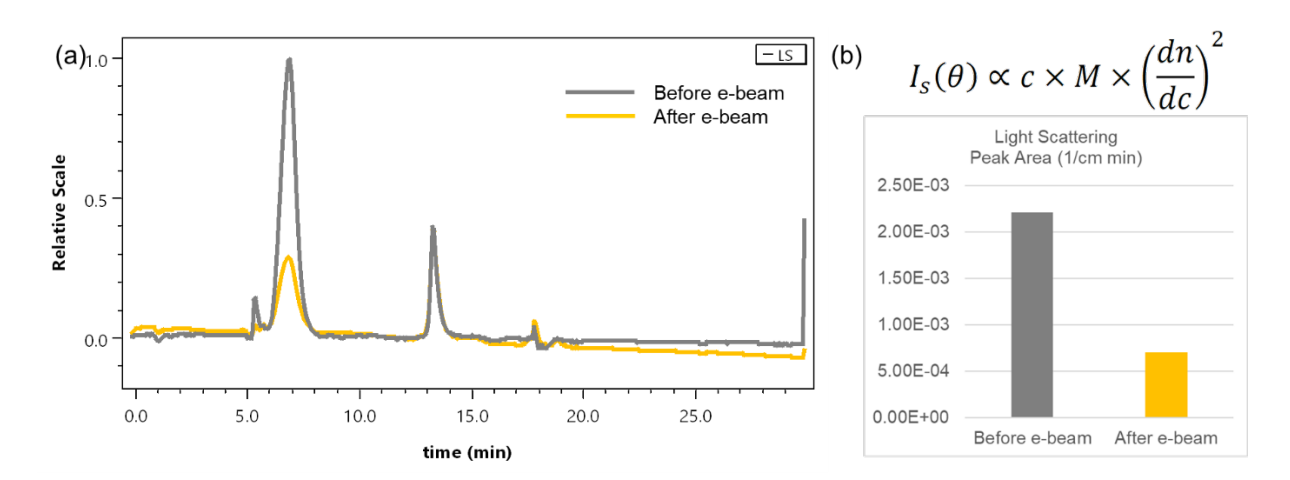


Figure S7. RPLC-MALS study of PNP-2-10 hydrogel before and after e-beam treatment. (a) Light scattering chromatograms (90 degree) of the PNP-2-10 hydrogel before (grey) and after (yellow) e-beam treatment. (b) Equation of MALS detector working principle and summary of light scattering area of HPMC-C₁₂ in the PNP-2-10 hydrogel before (grey) and after (yellow) e-beam.

The scattered light intensity I_s is proportional to mass concentration c (0.04 mg/mL for HPMC- $_{12}$ in the analysis), molecular weight M, and the square of dn/dc (refractive index increment). The HPMC- C_{12} peak area in the e-beam sterilized PNP- $_{2}$ -10 hydrogel showed $_{2}$ times decrease compared with the peak area in the untreated PNP- $_{2}$ -10 hydrogel. Given that the mass concentration and dn/dc values before and after e-beam remained the same, the peak area reduction was proportional to the molecular weight decrease according to the equation of the MALS detector principle. $_{2}$

10. Analysis of Polymer Degradant by RPLC Coupled with a High Resolution Mass Spectrometer

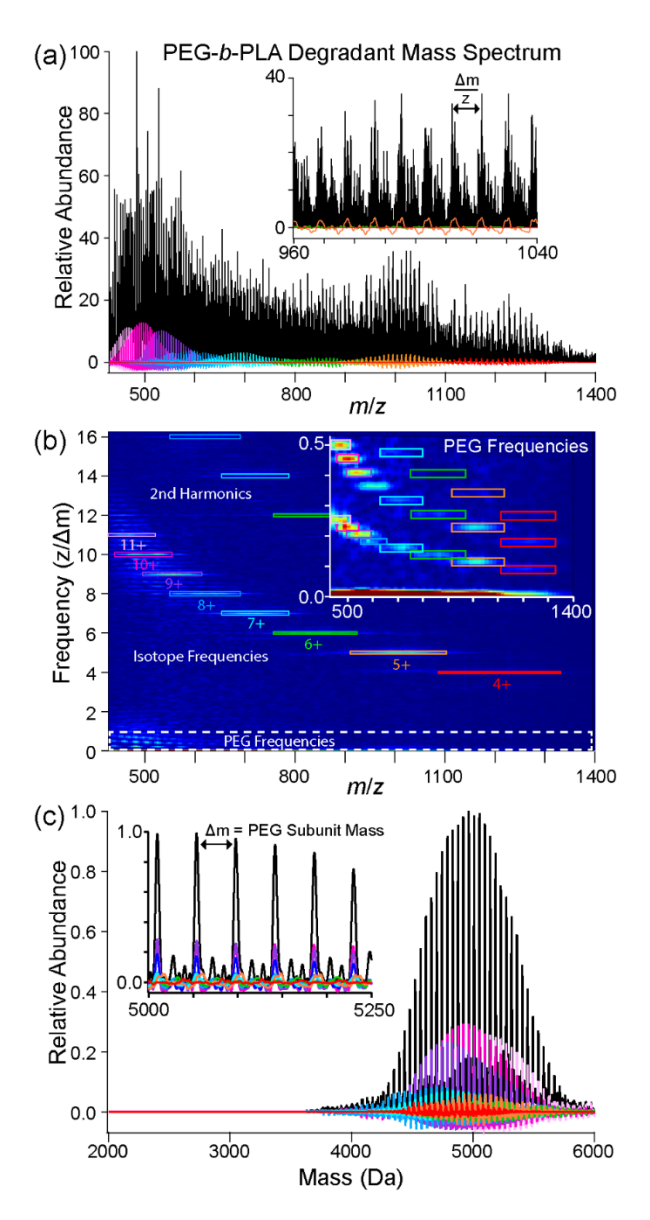


Figure S8. iFAMS deconvolution of the PEG-*b*-PLA degradant mass spectrum using Gábor Transform (GT). ⁷ Fourier analysis converts periodic peak distributions from the mass spectrum (a, inset) into distinct features in frequency (transforming $\Delta m/z \rightarrow z/\Delta m$). GT is a windowed-Fourier transform technique that enables localization of frequency information from the mass spectrum (a) in a 2D spectrogram (b). Since the mass spectrum is isotopically resolved, GT identifies signal at integer frequencies (corresponding to isotope spacings, $\Delta m \approx 1$ Da) in addition to lower frequencies corresponding to the PEG subunit ($\Delta m \approx 44.05$ Da) (b, inset), simplifying charge distribution assignment of the multiply charged polymer ions. Inverse Gábor Transform of the PEG subunit frequencies and their harmonics (b, colored boxes) back to m/z generates charge-specific mass distributions with subunit resolution (a, colored spectra). The charge-specific mass distributions are normalized for charge and combined into a total mass

reconstruction of the identified polymer charge series (c), and the repeated subunit mass can be confirmed from each charge state (c, inset).

References:

- (1) Meany, E. L.; Andaya, R.; Tang, S.; Kasse, C. M.; Fuji, R. N.; Grosskopf, A. K.; d'Aquino, A. L.; Bartoe, J. T.; Ybarra, R.; Shelton, A.; Pederson, Z.; Hu, C.; Leung, D.; Nagapudi, K.; Ubhayakar, S.; Wright, M.; Yen. C.-H.; Appel, E. A. Injectable Polymer-Nanoparticle Hydrogel for the Sustained Intravitreal Delivery of Bimatoprost. *Adv. Therap.* **2022**, *6*, 2200207.
- (2) Bouvier, E. S. P.; Koza, S. M. Advances in Size-Exclusion Separations of Proteins and Polymers by UHPLC. *Trends Anal. Chem.* **2014**, *63*, 85-94.
- (3) Li, Y.; Shen, H.; Lyons, J. W.; Sammler, R. L.; Brackhagen, M.; Meunier, D. M. Size-Exclusion Chromatography of Ultrahigh Molecular Weight Methylcellulose Ethers and Hydroxypropyl Methylcellulose Ethers for Reliable Molecular Weight Distribution Characterization. *Carbohydr. Polym.* **2016**, *138*, 290-300.
- (4) Maikawa, C. L.; Sevit, A.; Lin, B.; Wallstrom, R. J.; Mann, J. L.; Yu, A. C.; Waymouth, R. M.; Appel, E. A. Block Copolymer Composition Drives Function of Self-Assembled Nanoparticles for Delivery of Small-Molecule Cargo. *J. Polym. Sci. A Polym. Chem.* **2019**, *57*, 1322-1332.
- (5) Huglin, M. B. Specific Refractive Index Increments of Polymer Solutions. Part I. Literature Values. *J. Appl. Polym. Sci.* **1965**, 9, 3963-4001.
- (6) Rubinstein, M.; Colby, R. H. *Polymer Physics*; Oxford University Press New York, 2003.
- (7) Cleary, S. P.; Prell, J. S. Liberating Native Mass Spectrometry from Dependence on Volatile Salt Buffers by Use of Gabor Transform. *ChemPhysChem* **2019**, *20*, 519-523.